Desert pavement–coated surfaces in extreme deserts present the longest-lived landforms on Earth

Ari Matmon†
The Institute of Earth Sciences, Hebrew University of Jerusalem, Givat Ram, Jerusalem 91904, Israel

Ori Simhai
The Institute of Earth Sciences, Hebrew University of Jerusalem, Givat Ram, Jerusalem 91904, Israel, and Geological Survey of Israel, 30 Malkhe Israel Street, Jerusalem 95501, Israel

Rivka Amit
Geological Survey of Israel, 30 Malkhe Israel Street, Jerusalem 95501, Israel

Itai Haviv
The Institute of Earth Sciences, Hebrew University of Jerusalem, Givat Ram, Jerusalem 91904, Israel

Naomi Porat
Geological Survey of Israel, 30 Malkhe Israel Street, Jerusalem 95501, Israel

Eric McDonald
Desert Research Institute, 2215 Raggio Parkway, Reno, Nevada 89512, USA

Lucilla Benedetti
Centre Européen de Recherche et d'Enseignement des Géosciences de l'Environnement, Europôle Méditerranéen de l'Arbois, BP 80, Aix en Provence, cedex 04, 13545, France

Robert Finkel
Lawrence Livermore National Laboratory, 7000 East Avenue, Livermore, California 94550, USA

ABSTRACT

All exposed rocks on Earth's surface experience erosion; the fastest rates are documented in rapidly uplifted monsoonal mountain ranges, and the slowest occur in extreme cold or warm deserts—millennial submeter-scale erosion may be approached only in the latter. The oldest previously reported exposure ages are from boulders and clasts of resistant lithologies lying at the surface, and the slowest reported erosion rates are derived from bedrock outcrops or boulders that erode more slowly than their surroundings; thus, these oldest reported ages and slowest erosion rates relate to outstanding features in the landscape, while the surrounding landscape may erode faster and be younger. We present erosion rate and exposure age data from the Paran Plains, a typical environment in the Near East where vast abandoned alluvial surfaces (10^2–10^4 km^2) are covered by well-developed desert pavements. These surfaces may experience erosion rates that are slower than those documented elsewhere on our planet and can retain their original geometry for more than 2 m.y. Major factors that reduce erosion converge in these regions: extreme hyperaridity, tectonic stability, flat and horizontal surfaces (i.e., no relief), and effective surface armoring by a clast mosaic of highly resistant lithology. The ^{10}Be concentrations in amalgamated desert pavement chert clasts collected from abandoned alluvial surfaces in the southern Negev, Israel (representing the Sahara-Arabia Deserts), indicate simple exposure ages of 1.5–1.8 Ma or correspond to maximum erosion rates of 0.25–0.3 m m.y.$^{-1}$. The ^{36}Cl in carbonate clasts, from the same pavement, weathers faster than the chert and yields simple exposure ages of 430–490 ka or maximum erosion rates of 0.7–0.8 m m.y.$^{-1}$. These ages and rates are exceptional because they represent an extensive landform. The ^{10}Be concentrations from samples collected at depth and optically stimulated luminescence (OSL) dating reveal a two-stage colluvial deposition history followed by eolian addition of 40 cm of silt during the past 170 k.y. Our results highlight the efficiency of desert pavement armor in protecting rocks from erosion and preserving such geomorphic surfaces for millions of years.

INTRODUCTION

Stable gravelly alluvial surfaces in hyperarid environments are characterized by Reg soil formation and cover ~20% of the Middle East deserts, North Africa, and other extremely arid regions of the world (Dan et al., 1982; Gerson, 1982). Most of the Reg soils are salty, dust-rich, and capped by a mosaic of pebbly clasts that form desert pavements (e.g., Rabikovitch et al., 1957; Dan et al., 1982; Cooke et al., 1993; Amit et al., 1993; McFadden et al., 1987, 2000; McDonald et al., 2003). Such pavements

†E-mail: arimatmon@cc.huji.ac.il.

GSA Bulletin; May/June 2009; v. 121; no. 5/6; p. 688–697; doi: 10.1130/B26422.1; 4 figures; 5 tables.

form within <50 k.y. (e.g., Amit and Gerson, 1986; Amit et al. 1993; McFadden et al., 2000). The desert pavement clasts reside at the surface during soil formation, while fine-grained dust infiltrates underneath the clasts and shift them upward (McFadden et al., 1987, 2000; Gerson and Amit, 1987; Wells et al., 1995). Weathering causes the breakdown of original clasts into well-sorted, homogeneously pebble-sized desert pavement clasts. Internal fractures or discontinuities are nearly absent in these smaller clasts. Therefore, the rate at which they weather drops dramatically, especially in hyperarid environments, where soil water and organic material are absent and clasts are composed of fine-grained silicates.

Under unique conditions of long-term hyperaridity and the absence of soil and vegetation for an extended period, desert pavement will not be recycled. In such settings, the subsoil sediment, the desert pavement, and by inference the surface itself will have similar ages. Under such conditions, desert pavement clasts are continuously exposed at the surface and do not erode—two very important features when considering cosmogenic age dating. In this study, we present numeric data documenting the extreme longevity of desert pavement and the surface on which it lies in a hyperarid and tectonically stable region.

The use of cosmogenic isotopes to determine exposure ages and erosion rates (Lal, 1988; Bierman, 1994; Gosse and Phillips, 2001) of bedrock, alluvial, colluvial, and glacial geomorphic surfaces has yielded a large range of ages and rates (e.g., Bierman and Caffee, 2001, 2002; Bierman and Turner, 1995; Stone et al., 2005; Daeron et al., 2004; Matmon et al., 2005a, 2005b, 2006; Briner et al., 2001, 2002; Siame et al., 1997; Fig. 1). Because the buildup of cosmogenic isotope concentrations in exposed rocks and surfaces is very sensitive to erosion (Gosse and Phillips, 2001), exposure age dating is generally limited to 10^3–10^5 yr. Therefore, although alluvial surfaces (terraces and fans) are routinely dated using cosmogenic isotopes (e.g., Gosse et al., 2003a, 2003b, 2004; Phillips et al., 1998), only in rare cases do conditions enable the determination of surface exposure ages that are $>10^6$ yr. Several studies have dated extremely old landscapes by collecting and analyzing selected clast samples that were lying at the surface (e.g., Dunai et al., 2005; Ewing et al., 2006). These collected samples are generally different from the typical clast covering the surface. Such a sampling strategy leaves important questions unanswered: does the exposure age of the selected samples represent the actual age of the surface? Are average rates of surface processes as slow as indicated by the selected few samples? A hint to the answer is found in some studies (i.e., Dunai et al., 2005) that show a difference of one to two orders of magnitude in cosmogenic nuclide concentration between selected resistant clasts and alluvial sediments. This is despite the fact that such a difference implies that some parts of the geomorphic system are eroding much faster than others and that the antiquity of the landscape cannot be characterized by selected resistant clast and boulder samples.

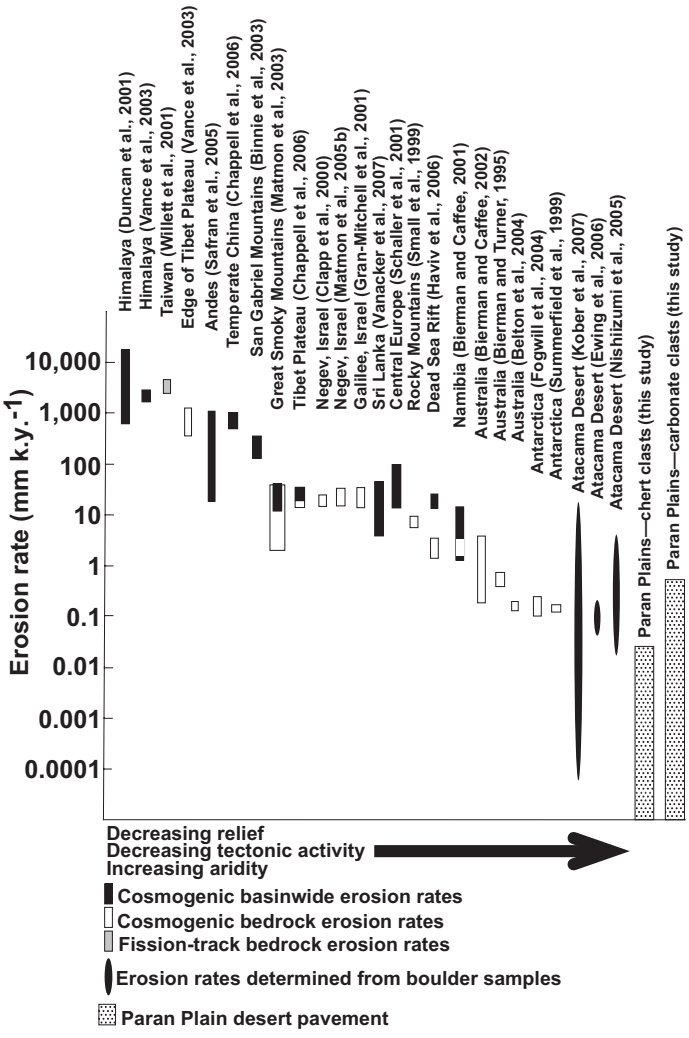

Figure 1. Compilation of erosion rates calculated from cosmogenic concentrations in bedrock, boulder, and sediment samples from selected studies. Gray box—Taiwan erosion rates (Willett et al., 2001) from fission-track data. The fastest erosion rates are recorded in the steepest and tectonically most active mountain belts. The slowest rates are from the cold and warm hyperarid regions of the world. Results from other studies would fall between these extremes. A similar pattern was shown by Milliman and Syvitski (1992) based on modern river sediment yield. Although erosion rates obtained for the Paran Plains (dotted boxes) and for the Atacama Desert overlap, the Atacama samples were all collected from individual resistant boulders and clasts lying at the surface. These samples most likely do not represent the age or the typical erosion rate of the surface from which they were collected. In contrast, the amalgamated clast samples of the Paran Plains' desert pavement represent its age better. The maximum erosion rate of the surface of Paran Plains was separately calculated for chert clasts and carbonate clasts.

STUDY AREA

The Negev Desert of southern Israel is part of the global desert belt that includes the Sinai, Arabia, and Sahara Deserts. The Paran Plains lie in the hyperarid (<50 mm/yr) southern Negev, ~35 km west of the Dead Sea fault (Fig. 2). Overlain mainly by a veneer of alluvium, the Paran Plains were formed in the Pliocene,

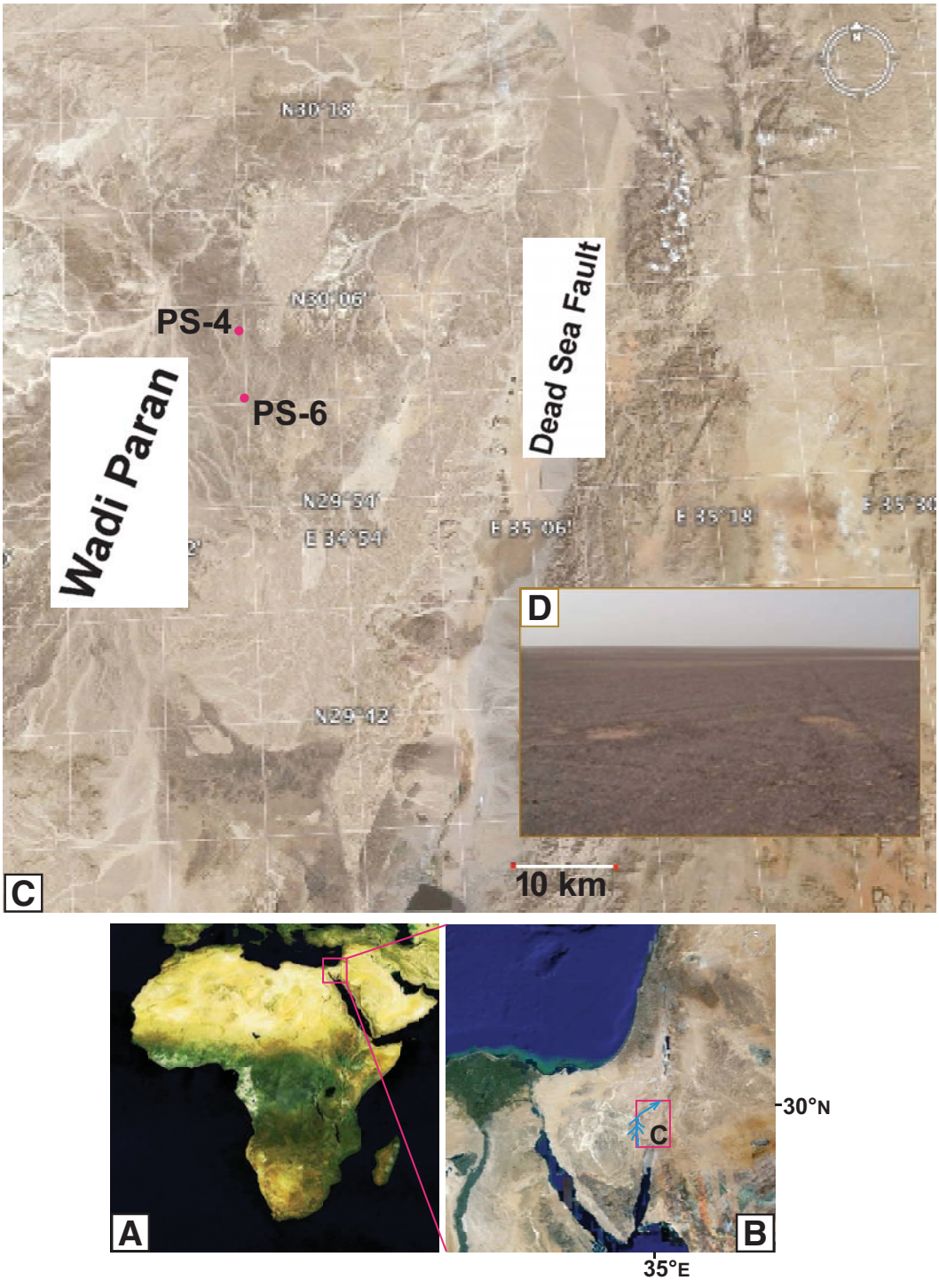

Figure 2. (A) Location of study area (red box) in the Northern Hemisphere deserts of the Sahara and Arabia. (B) The Paran drainage system (blue lines) is the largest drainage system in the Negev (~3,840 km^2). It drains from the uplifted Sinai shoulders of the Red Sea–Gulf of Aqaba northward to the Dead Sea basin. (C) Satellite image of the Paran Plains. Brown patches represent desert pavement-coated surfaces. Bright patches and lines represent active drainages and valleys. Research trenches (red dots) into this extremely flat geomorphic surface indicate that the northern site (PS-4) is composed of angular colluvial sediment and the southern site (PS-6) is composed mostly of alluvial sediment. Sediment in the northern site was delivered from nearby outcrops of Senonian chert. Thus, inheritance and transport time were relatively constant. (D) A typical appearance of the landscape in the study area. A well-developed desert pavement covers ~85% of the surface. The region is tilted <1° to the NNW.

when the Wadi Paran drainage system developed in response to the initial subsidence of the Dead Sea basin (Avni, 1991; Avni et al., 2000). Despite their relative proximity to the Dead Sea fault, the Paran Plains are hardly influenced by Quaternary tectonics and are tilted at only a fraction of a degree toward the main stem of Wadi Paran (Avni, 1991; Avni et al., 2000). These surfaces are capped by a continuous and mature desert pavement (>80% cover) composed of chert clasts and a minor amount of limestone and dolomite pebbles. This desert pavement covers the entire Paran Plains (Fig. 2). Beneath the desert pavement, the sediment is generally composed of angular clasts typical of a pediment or a bajada. The gravelly section is homogeneous, without significant changes in deposition type or lithologic composition and without noticeable unconformities. The upper 40 cm consist of fine-grained material, mostly of eolian origin (Fig. 3). In some locations, the sediment includes horizons of rounded carbonate pebbles, indicating the inclusion of alluvial material. In places where these carbonate pebbles are exposed at the surface, they follow the trace of the currently flat and subdued original depositional bars.

METHODS

Cosmogenic Isotopes

We measured cosmogenic ^{10}Be concentrations in seven amalgamated samples and ^{36}Cl concentrations in two samples to determine the history of the Paran Plain alluvial surface. We collected four amalgamated desert pavement samples from two sites 8 km apart. These samples included one amalgamated chert sample from a northern site and three amalgamated samples, one chert and two carbonate (collected several tens of meters from each other), from a southern site (Table 1; Fig. 2). For a good representative sample, 25–40 clasts are enough to get a reproducible mean concentration in a geomorphic system (Repka et al., 1997). We amalgamated tens to >100 of desert pavement clasts in our samples to ensure a cosmogenic nuclide concentration that represents the average dosing, and thus exposure, of the entire Paran Plains desert pavement. The heavily varnished chert clasts range in size between 2 and 5 cm. The rounded carbonate clasts are somewhat larger (2–15 cm) and are slightly to moderately pitted. We hypothesize that in this unique case, where the desert pavement has not been disturbed since formation, the exposure age of the chert clasts (>95% of the desert pavement clasts) also represents the actual age of the geomorphic surface. Since most carbonate pebbles were derived from bars, we expect differences in the exposure history between the chert and the carbonate clasts because of bar relief reduction over time. In addition to the desert pavement samples, five amalgamated chert samples were collected at depths of 110–190 cm from a 2-m-deep trench at the northern site (Table 2; Fig. 3).

Samples for cosmogenic ^{10}Be were processed following Bierman and Caffee (2001) and Stone

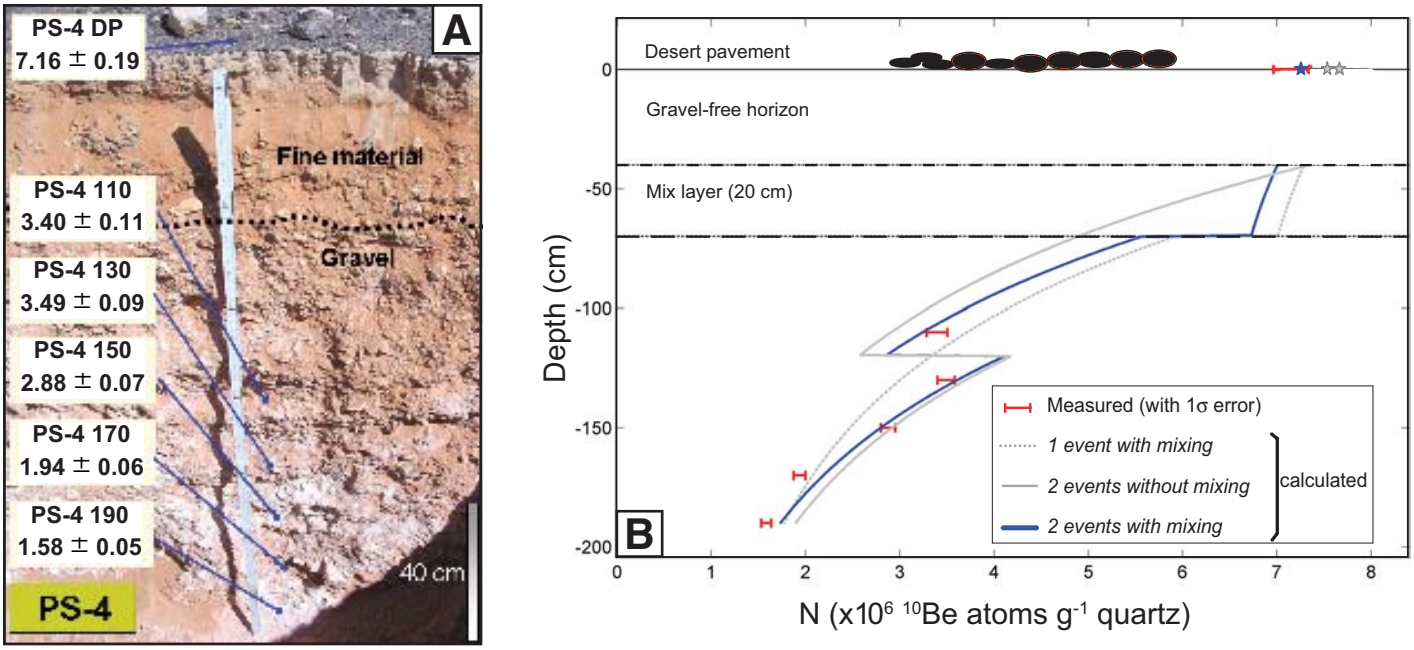

Figure 3. (A) Soil profile exposed in trench PS-4. Sediment in the lower part is composed of angular clasts typical of a pediment or a bajada. The gravelly section is homogeneous without significant changes in sedimentology and without noticeable unconformities. The upper 40 cm of the profile consist of very fine sand to clay dust. Notice the brighter, 5–10-cm-thick columnar Av horizon capped by the tightly arranged single-layer desert pavement composed of heavily varnished, 2–5 cm platy chert clasts. Large cobbles on the pavement were extracted from the section during trench excavation. Several varnished chert clasts can be seen within the clast-free horizon left of the measuring tape. Concentrations of ^{10}Be (in 10^6 atoms g^{-1} quartz with 1σ analytical error) generally decrease with increasing depth, apart from a slight increase from 110 cm to 130 cm (Table 1). (B) Model results showing measured ^{10}Be concentrations (red bars) and three end member scenarios of ^{10}Be profiles (Table 5). Stars represent the calculated concentrations in amalgamated surface desert pavement samples. The "with mixing" term refers to scenarios in which pavement clasts were derived from a 20-cm-thick mixed layer of the second depositional gravel. The "two events with mixing" scenario yielded the best fit. The age obtained for the first deposition event in this scenario is 2.05 Ma (Table 5). Inheritance of 320,000 atoms g^{-1} quartz is equivalent to an average erosion rate of 14 mm k.y.$^{-1}$. Dust accumulation at a constant rate was considered in all scenarios, starting from 170 ka to present based on optically stimulated luminescence (OSL) ages (Table 4).

et al. (1996) for ^{36}Cl. Accelerator Mass Spectrometry (AMS) analyses were performed at Lawrence Livermore National Laboratory. We used Stone (2000) for scaling production rate and a sea-level high-latitude (SLHL) production rate of 5.2 atoms per g quartz per year for ^{10}Be (Stone, 2000). The ^{10}Be model ages were calculated using both a decay constant of 4.62×10^{-7} yr^{-1} (corresponding to a half-life of 1.5 m.y.) and 5.1×10^{-7} yr^{-1} (corresponding to a half-life of 1.36 m.y.). For ^{36}Cl, we used an SLHL production rate of 54 atoms per g Ca per year for total production from Ca, partitioned between spallation (48.8 ± 3.4 atoms per g Ca per year) and muon capture reactions (5.2 ± 1.2 atoms per g Ca per year) as described by Stone et al. (1996, 1998). None of the samples contained significant amounts of K, Fe, or Ti (Table 3A). Production rates by thermal and epithermal neutron capture were calculated using the method of Phillips et al. (2001). Chemical analyses of carbonate samples were performed at the inductively coupled plasma–mass spectrometry (ICP-MS) facility, Israel Geological Survey (Table 3).

TABLE 1. CHERT SAMPLES FROM PARAN PLAINS

Sample name	Site*	Depth (cm below surface)	Site production rate (atoms g^{-1} qtz yr^{-1})†	Concentration (×10^6 atoms ^{10}Be g^{-1} qtz)§	Simple exposure age (×10^6 yr)#	Maximum erosion rate (m m.y.$^{-1}$)#
PS-6 DP	PS-6	0 (Surface)	6.8 ± 0.7	8.18 ± 0.22	1.8 ± 0.3	0.22 ± 0.04
PS-4 DP	PS-4	0 (Surface)	6.8 ± 0.7	7.16 ± 0.20	1.5 ± 0.2	0.3 ± 0.04
PS-4 110	PS-4	110	1.6 ± 0.2	3.40 ± 0.11		
PS-4 130	PS-4	130	1.2 ± 0.1	3.49 ± 0.09		
PS-4 150	PS-4	150	0.9 ± 0.09	2.88 ± 0.08		
PS-4 170	PS-4	170	0.8 ± 0.08	1.94 ± 0.06		
PS-4 190	PS-4	190	0.6 ± 0.06	1.58 ± 0.05		

*PS-4: 30.08°N, 34.79°E. PS-6: 30.02°N, 34.80°E. Elevation: 520 m asl.
†Propagated 10% error in production rate.
§Analytical 1σ error.
#Analytical error and production rate uncertainty.

Optically Stimulated Luminescence (OSL) Ages

Luminescence methods date the last exposure of mineral grains to sunlight or high temperature (Aitken, 1998). These methods use signals that accumulate in minerals as a result of natural ionizing radiation. Only several minutes of light exposure are necessary to zero the OSL signal in quartz (Aitken, 1998). After a resetting event and burial, the signal grows as a function of time and environmental radiation, and therefore it can be used to estimate the time elapsed since the mineral underwent an event of transport, exposure, deposition, and burial.

We collected 13 samples for OSL dating from depths that range between 80 cm and 1 cm below the surface (Table 4). Due to the sensitivity of the luminescence signals, samples for dating were collected in the dark. A layer of tens of centimeters was scraped back from the vertical face in the dark before collecting the sample to avoid the inclusion of bleached material in the sample. Samples were placed immediately in light-tight bags, and all subsequent laboratory procedures were carried out under subdued orange light. Quartz (fine sand size) was separated and purified from the bulk sediment using standard laboratory procedures (Zilberman et al., 2000). Annual gamma and cosmic dose rates were measured in the field using a portable gamma scintillator. Alpha and beta dose rates were calculated from the concentrations of the radioelements U, Th, and K in the sediment. Luminescence measurements were carried out on a Risó D-12 TL/OSL reader. Equivalent doses (D_e) were determined using the single aliquot regenerative dose (SAR) protocol (Murray and Wintle, 2000); the D_e used for age calculations was averaged from 10 to 12 aliquots.

Model

Profile model exposure ages were calculated using the formula from Brown et al. (1998):

$$N = \frac{P}{\rho\varepsilon\Lambda^{-1} + \lambda}(1 - e^{-(\rho\varepsilon\Lambda^{-1} + \lambda)t}) + N(0)e^{-\lambda t}, \quad (1)$$

where N is the measured concentration of the cosmogenic nuclide in atoms per g quartz, P is the total surface production rate of the cosmogenic nuclide in atoms per g quartz per year, ρ is the density of the consolidated sediment (2.4 g cm^{-3}) or fine eolian material (1.6 g cm^{-3}), ε is the erosion rate of the clasts in cm yr^{-1}, Λ is the attenuation depth of neutrons (165 g cm^{-2}), t is the exposure age in years, $N(0)$ is the inherited cosmogenic nuclide concentration in atoms per g quartz at the time of deposition, and λ is the cosmogenic nuclide decay constant (4.62×10^{-7} yr^{-1} or 5.1×10^{-7} yr^{-1}). We assumed similar altitude and latitude to the present. Inheritance was an unbound parameter, and ε was designated as "0" due to the extreme resistance of chert clasts to erosion in this hyperarid environment.

The model objective was to find the exposure age (t) in the simplest possible scenario (i.e., minimum deposition events) yielding the best fit between measured and calculated concentrations. Calculated ^{10}Be concentrations (Nc) were compared with the measured ones (Nm) for all samples in each scenario to test the fit. The best fit was calculated using a chi-square test. The level of fit was calculated using:

$$\frac{(Nc_1 - Nm_1)^2}{\sigma_{m_1}^2} + \frac{(Nc_2 - Nm_2)^2}{\sigma_{m_2}^2} + \ldots \frac{(Nc_6 - Nm_6)^2}{\sigma_{m_6}^2}, \quad (2)$$

where "0" was the best result.

Production rates and exposure ages of PS-4 samples were calculated considering a few scenarios with different burial and shielding histories. The exposure age model considered inherited cosmogenic nuclide concentrations (N[0]), one or two depositional events, a time interval between the depositional events (*Dif*), and continuous dust accumulation since 170 ka (as indicated by the OSL ages). Thus, we considered increasing shielding depths to the samples, changing Equation 1 to –ε instead of ε, as well as using a lower density value (1.6 instead of

TABLE 2. CARBONATE SAMPLES FROM PARAN PLAINS

Sample name	Site*	Depth (cm below surface)	Site production rate (atoms g^{-1} rock yr^{-1})†	Concentration (×10^6 atoms ^{36}Cl g^{-1} rock)†	Simple exposure age (×10^5 yr)§	Maximum erosion rate (m m.y.$^{-1}$)§
PS-6 BAR	PS-6	0 (Surface)	29.8 ± 1.5	8.47 ± 0.11	4.6 ± 0.25	0.83 ± 0.045
PS-6 SWALE	PS-6	0 (Surface)	30.2 ± 1.6	8.89 ± 0.1	4.9 ± 0.26	0.75 ± 0.04

*See Table 1 for location of sites.
†Calculated following Stone et al. (1996, 1998) and Phillips et al. (2001). Analytical 1σ error.
§Analytical error and production rate uncertainty.

2.4 g cm^{-3} for the gravel) for the upper part of the section. The gradual accumulation of dust, starting at 170 ka and lasting to the present, adds to the total shielding of the depth samples, whereas dust that accumulated between 350 ka and 170 ka penetrated into the colluvial section and did not add to the total thickness, and thus shielding, of the samples. A 20 cm mixing layer from which desert pavement clasts were originally derived was also considered. Model output, t_{total}, describes the total time since initial deposition by optimizing parameters *Dif* and $N(0)$.

Field observations indicate that, periodically, a small number of varnish-coated desert pavement clasts sink into the clast-free eolian layer (Fig. 3). Thus, it is possible that on average each clast in the pavement spends some time at a depth of a few centimeters, thus reducing the overall average production rate of ^{10}Be in the clasts. We simulated this cycle as an average shielding of 10 cm of the desert pavement by eolian dust since it started to accumulate until the present.

TABLE 3A. CARBONATE SAMPLES: WHOLE-ROCK CHEMICAL COMPOSITION

Sample name	SiO_2 (wt%)	Al_2O_3 (wt%)	Fe_2O_3 (wt%)	TiO_2 (wt%)	CaO (wt%)	MgO (wt%)	MnO (wt%)	Na_2O (wt%)	K_2O (wt%)
PS6-Bar	0.5	<0.1	<0.1	<0.01	55.3	0.4	<0.01	<0.1	<0.1
PS6-Swale	0.6	0.1	0.1	<0.01	55.1	0.4	<0.01	<0.1	<0.1

Sample name	P_2O_5 (wt%)	Li (ppm)	B (ppm)	Cr (ppm)	Sm (ppm)	Gd (ppm)	Ba (ppm)	Th (ppm)	U (ppm)
PS6-Bar	<0.1	0.6	<10	8	0.5	0.1	725	0.1	0.8
PS6-Swale	<0.1	0.6	<10	8	0.8	0.2	1350	0.2	0.9

TABLE 3B. CARBONATE SAMPLES: DISSOLVED FRACTION CHEMICAL COMPOSITION

Sample name	Ca (mg/L)	Mg (mg/L)	K (mg/L)	Na (mg/L)	Sr (mg/L)	Fe (mg/L)	Ti (mg/L)	Ba (mg/L)	Mn (mg/L)
PS-6 Bar	29000	155	0.7	7	13	3	0.6	13	1.7
PS-6 Swale	27500	150	0.9	7	13	2	0.6	18	1.9

RESULTS AND DISCUSSION

Temporal Framework and Soil Characteristics of the Paran Plains

The Pliocene-Pleistocene history of the Paran drainage system and its relation to Dead Sea transform tectonic activity have been extensively studied (e.g., Avni, 1991; Avni et al., 2000). Although most are semiquantitative studies, they present the temporal framework for the morphotectonic development of this region. The alluvial surfaces are younger than the Miocene Hazeva Formation (Avni et al., 2000). This formation includes mainly alluvial sediments derived from the trans-Jordan highlands and transported to the Mediterranean prior to the subsidence of the Arava Valley along the Dead Sea transform (Garfunkel and Horovitz, 1966). The accepted age of the top most sediments of the Hazeva Formation is 10–14 Ma (Zilberman and Avni, 2006), although others (e.g., Calvo and Bartov, 2001) have suggested a much younger age of ca. 6 Ma. The Paran Plain alluvial surface is older than the widespread red-bed unit in the central Negev. This unit contains fauna indicative of the early to middle Pleistocene and Acheulian tools estimated as 1.4–2 Ma (Ginat et al., 2002). Together, these age boundaries agree with earlier suggestions (e.g., Garfunkel and Horovitz, 1966) of Pliocene age (2–5 Ma) for the sediments deposited by the ancient Paran drainage system.

The age of the development of drainage systems flowing from the Negev into the Dead Sea basin is obviously constrained by the initial formation of the Dead Sea as a regional base level at 3–8 Ma (e.g., Steinitz and Bartov, 1991). The activity of the ancient Paran drainage system and the deposition of the Paran Plains sediments are therefore bounded between 6 and 1.4 Ma. From field geomorphic relationships, we estimated that Paran Plains were abandoned during the later stages of this age range.

With this proposed old age, the soil that has developed since abandonment of the Paran Plains should present very well-developed arid soils. The Reg soils of the Paran Plains include a very dense (>80%) desert pavement cover (Figs. 2 and 3). Salt fracturing of clasts near the surface (Amit et al., 1993) is absent, suggesting that all possible fracturing has already occurred, and clasts have reached their minimal size. The Av horizon is extremely thick for this region (5–10 cm), as is the clast-free B-horizon (~40 cm) (Fig. 3). The presence of a weak Bk-horizon, which is replaced later by a By-horizon, implies a cumulative soil that has experienced long-term climatic changes but has not eroded (Amit et al., 2006). Amit et al. (2006) suggested that climatic conditions in the southern Negev during the past 300 k.y. and perhaps since the early Pleistocene have been too arid for the formation of soil calcic horizon. These authors also suggested that such Bk-horizons in flat abandoned alluvial surfaces are probably late Pliocene to early Pleistocene in age, conforming with the geologic framework.

Desert Pavement and Paran Surface Exposure Ages

Debate is ongoing as to the justification of using desert pavements as surface age indicators. For example, in the southwestern United States, Quade (2001) argued that desert pavements might not serve as good surface age indicators

TABLE 4. OPTICALLY STIMULATED LUMINESCENCE (OSL) DATA

Sample name	Depth (cm)	Avg. depth (cm)	Moisture (%)	K (%)	Th (ppm)	U (ppm)	External dose (Gy/k.y.) α	β	γ	Cosmic*	Dose rate (Gy/k.y.)	Paleodose (Gy)	Age (ka)
PS-40	0–2	1	0.6	0.79	5.9	2.6	0.010	1.025	0.758	0.307	2.088 ± 0.027	1.545 ± 0.053	0.7 ± 0.2
PS-41	2–5	3.5	1.3	0.79	5.9	2.6	0.012	1.034	0.758	0.284	2.088 ± 0.027	6.117 ± 0.209	3 ± 0. 7
PS-42	5–8	6.5	1.5	0.73	3.9	1.8	0.009	0.846	0.560	0.275	1.670 ± 0.028	19.71 ± 0.67	12 ± 5
PS-43	8–12	10	1.9	0.69	4.3	2.5	0.012	0.919	0.785	*	1.822 ± 0.027	39.90 ± 1.60	22 ± 75
PS-44	20–14	17	2.1	0.68	4.1	2.1	0.090	0.848	0.785	*	1.642 ± 0.082	68.79 ± 2.36	42 ± 125
PS-45	27–20	23.5	2.1	0.58	3.8	2	0.010	0.764	0.542	0.240	1.536 ± 0.023	79.87 ± 2.74	52 ± 17
PS-46	32–28	30	2.1	0.33	2.9	2.2	0.010	0.593	0.462	0.229	1.213 ± 0.024	109.4 ± 3.7	90 ± 22
PS-47	40–34	37	1.8	0.33	2.9	2.2	0.008	0.588	0.785	*	1.280 ± 0.024	165.1 ± 5.7	129 ± 40
PS-47A	38–42	40	1.8	0.17	1.7	2.5	0.008	0.486	0.400	0.219	1.113 ± 0.023	188.1 ± 6.5	169 ± 52
PS-47B	52–48	50	1.5	0.14	1.3	1.9	0.006	0.377	0.307	0.210	0.901 ± 0.023	186.1 ± 6.4	207 ± 34
PS-48	62–58	60	1.5	0.29	2.8	2	0.009	0.536	0.425	0.203	1.172 ± 0.024	201.6 ± 6.9	172 ± 49
PS-48A	72–68	70	1.2	0.13	1.2	1.5	0.005	0.315	0.255	0.196	0.772 ± 0.023	275.6 ± 9.5	357 ± 40
PS-49	82–78	80	1.2	0.12	1.3	2	0.008	0.379	0.313	0.200	0.878 ± 0.250	273.1 ± 9.4	311 ± 26

*Cosmic radiation is included in the γ, which was measured in the field.

since they could be disrupted by the expansion of vegetation into barren regions during glacial periods and then rejuvenated later during arid phases. On the other hand, Valentine and Harrington (2006), for example, made observations indicating the progressive maturity of pavements and their suitability as age indicators. Pelletier et al. (2007) attempted to reconcile these contradicting explanations with a numeric model in which pavements develop and mature with time and at the same time rejuvenation cycles affect, in a minor way, their level of maturity.

In the Paran Plains, all our cosmogenic samples yielded high cosmogenic nuclide concentrations that testify to their antiquity. Two pavement chert samples yielded ^{10}Be concentrations of 7.16 ± 0.19 × 10^6 atoms g^{-1} quartz and 8.18 ± 0.22 × 10^6 atoms g^{-1} quartz (Table 1; Fig. 3). The carbonate samples yielded ^{36}Cl concentrations of 8.89 ± 0.1 × 10^6 atoms g^{-1} rock and 8.47 ± 0.11 × 10^6 atoms g^{-1} rock (Table 2). At depth, ^{10}Be concentrations range between 1.58 ± 0.05 × 10^6 and 3.49 ± 0.09 × 10^6 atoms g^{-1} quartz (Fig. 3; Table 1). Concentrations of ^{10}Be in the depth samples generally decrease with increasing depth, apart from a slight increase from 110 cm to 130 cm.

The cosmogenic nuclide concentrations in the desert pavement chert samples imply a straightforward interpretation. The ^{10}Be concentrations of the chert pavement samples correspond to *simple* exposure ages of 1.5 ± 0.2 Ma and 1.9 ± 0.3 Ma when erosion is considered to be zero. These ages were calculated using a site surface production rate of 6.8 ± 0.7 atoms g^{-1} yr^{-1}, assuming continuous exposure and no erosion. These ^{10}Be exposure ages were calculated using the more commonly used decay constant (λ) of ^{10}Be (4.62 × 10^{-7} yr^{-1}, corresponding to $\tau_{1/2}$ = 1.5 m.y.) and considering the current altitude of 520 m above sea level. Simple exposure age calculations with a decay constant of 5.1 × 10^{-7} yr^{-1} ($\tau_{1/2}$ = 1.36 m.y.; Nishiizumi et al., 2007; Fink and Smith, 2007) yielded pavement ages that range between 1.5 ± 0.2 Ma and 2.0 ± 0.4 Ma. Thus, the most conservative desert pavement age is ≥1.5 Ma. The similarity of ^{10}Be desert pavement ages at the two sites contributes to the reliability of ages. The ^{10}Be concentrations in the desert pavement samples also correspond to maximum erosion rates that range between 0.22 and 0.3 m $m.y.^{-1}$. When using scaling factors of Dunai (2000), simple exposure ages of the desert pavement samples are longer and steady state erosion rates are slower. These erosion rates would imply minimum surface exposure ages that exceed 5 Ma. These ages are unrealistic considering our geologic knowledge and the temporal framework for the morphotectonic development of the Negev (Avni et al., 2000). Therefore, although these maximum erosion rates are extremely slow, the actual rates must be even slower.

The measured concentrations of ^{36}Cl in the amalgamated carbonate samples (PS6BAR and PS6SWALE) correspond to simple exposure ages (considering zero erosion) of 460–490 ka or to steady-state time-independent erosion rates of 0.75–0.83 m $m.y.^{-1}$. Such erosion rates imply a minimum exposure age of the carbonate clasts in the desert pavement of 1 Ma.

Exposure ages and erosion rates calculated from the chert clasts are different than those calculated from the carbonate clasts, even though they all reside in the same pavement. This difference must be considered. It can be seen, both at the surface and in the trenches, that chert clasts are distributed fairly evenly among bars and swales. On the other hand, the larger carbonate clasts are concentrated in patches following the ghosts of original depositional bars (Fig. 4). We assume that, originally, the carbonate pebbles were concentrated mainly in bars, since they are, on average, larger. During the first few 10^4–10^5 yr after the abandonment of this ancient alluvial surface, clasts were transported from bars to swales (e.g., Matmon et al., 2006). During the process of material diffusion from bars to swales, chert clasts accumulated at the surface, remained there, and desert pavement began to develop. The silicate composition of the chert ensured the high resistance of the clasts to weathering and erosion. Thus, chert was added to the surface but not removed from it. Its average cosmogenic dosing is controlled by a large fraction of clasts that were exposed during the initial stages of this process. On the other hand, carbonate pebbles, derived mainly from bars, also accumulated at the surface, but they were slowly weathered by dissolution. Thus, carbonate pebbles were removed as well as continuously and laterally added to the surface pavement from the bars. Therefore, the contribution of old and heavily dosed pebbles to the average dosing of carbonate clasts is diminished. The crucial consequence of this difference in process is that the average cosmogenic nuclide dosing of chert clasts is much greater than the average cosmogenic nuclide dosing of carbonate clasts; by inference, their average exposure age is longer. As the relief of bar and swale morphology was reduced, diffusion rate was also significantly reduced (or even ceased). Once the surface had been completely flattened (as it appears today), all clasts residing on the former bars and swales were dosed equally by cosmic radiation. The ability to distinguish bars and swales on the very flat surface today (Fig. 4) and the remarkable correspondence between the two amalgamated carbonate samples suggest that transport of clasts has not occurred since the stabilization of the surface. Nevertheless, the carbonate and chert clasts still have a memory of the difference in processes that affected them during the first 10^5 yr of the existence of the Paran Plains.

The ^{10}Be concentrations in amalgamated chert samples collected at depth cannot be interpreted in a straightforward manner and require modeling (Fig. 3). Model results agree with the surface samples and with our knowledge of the Pliocene-Pleistocene tectonic and landscape evolution of this region. The ^{10}Be concentrations of both surface and depth samples from the northern site were used jointly in a numerical model that describes the dosing of cosmogenic isotopes by cosmic radiation as a function of a three-step history of clastic and eolian deposition. The ^{10}Be concentration profile with depth in PS-4 trench suggests that sediment was deposited in two or more cycles and not in a single deposition event. This observation is supported by the poor fit between measured and calculated concentrations in the single event scenario (Fig. 3). Thus, we considered scenarios with two depositional events. The "concentration unconformity" at 120 cm depth was one of the conditions in the model that forced it to separate the deposition events at that depth, even though no field evidence for a break in deposition was found.

The history of eolian cover was determined by OSL ages in the dust fraction in samples collected from the upper 80 cm of the surface. From 80 to 40 cm, the dust filled the spaces between the chert clasts. Above 40 cm, the dust constitutes a separate unit. The oldest OSL age within the separate unit is 169 ± 52 ka. OSL ages range between 0.7 ka at 1 cm and 357 ka at 70 cm below the surface (Table 4). There is a gradual and almost linear increase in the OSL age from the surface to 40 cm depth, and below this depth, the results show a more irregular pattern.

In the best-fit model, an exposure age of 1.8 ± 0.3 Ma was calculated for the desert pavement. This age agrees with the simple exposure age calculation and, hence, verifies the assumptions of near-zero erosion of the exposed clasts and insignificant inheritance. The best-fit model (Table 5; Fig. 3) suggests two stages of clast deposition at 2.05 ± 0.3 Ma and 1.8 ± 0.3 Ma with a later eolian input. The model results suggest a predepositional dosing of ~320,000 atoms g^{-1} quartz. This dosing is equivalent to a late Pliocene source bedrock erosion rate of ~14 mm $k.y.^{-1}$ or a predepositional exposure age of ca. 48 k.y. The ^{10}Be exposure ages were also calculated using λ = 5.1 × 10^{-7} yr^{-1} ($\tau_{1/2}$ = 1.36 m.y.) and continuous exposure at an elevation of 520 m above sea level. These calculations

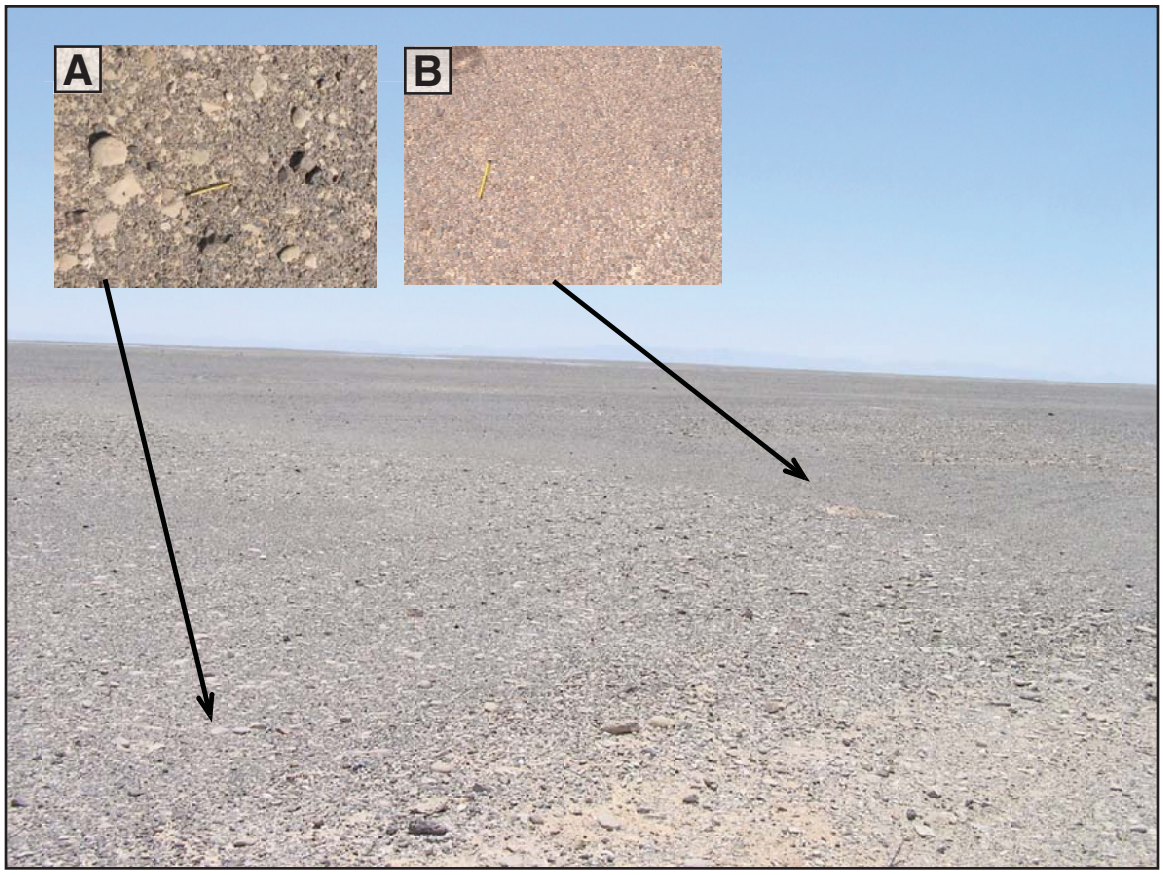

Figure 4. Bar and swale morphology of the ancient Paran Plains is still apparent on the flat surfaces. Bar ghosts contain carbonate pebbles as well as a majority of chert clasts (inset A). Swale ghosts contain only the mature and tightly arranged chert clasts (inset B). Presently, there is no relief between bars and swales.

TABLE 5. MODEL RESULTS FOR ^{10}Be SAMPLES IN SITE PS-4

^{10}Be half-life of 1.5 x 10^6 yr (λ = 4.62 x 10^{-7}); Elevation: 520 m asl					^{10}Be half-life of 1.36 x 10^6 yr (λ = 5.09 x 10^{-7}); Elevation: 520 m asl				
Dif (×10^5 yr)*	N_0 (×10^6 atoms g^{-1})	t_{total} (Ma)†	Fit	Scenario	Dif (×10^5 yr)*	N_0 (×10^6 atoms g^{-1})	t_{total} (Ma)†	Fit	Scenario
–	1.68	1.65	16.7	1 event with mixing (20 cm)	–	1.92	1.65	16.7	1 event with mixing (20cm)
2.5	0.48	1.80	7.0	2 events without mixing	2.5	0.76	1.75	7.0	2 events without mixing
2.5	0.32	2.05	3.6	2 events with mixing (20 cm)	3.5	0.40	2.35	3.78	2 events with mixing (20 cm)

Note: A 15% error is attributed to all ages; asl—above sea level.
*Time difference between first and second clast deposition. Pavement age equals the age of the second deposition.
†Time of first deposition.

yielded an older age of 2.35 Ma for initial deposition and a pavement age of 2.0 Ma.

After the Paran Plains surface was abandoned, at the latest 1.5–2.0 Ma, Reg soil and pavement began to develop. The diagnostic horizons of this soil (Birkeland, 1999) reflect continuous soil development during regional climatic changes. A calcic Bk horizon at a depth >1 m developed within the >2.0 Ma gravelly alluvium, and this implies root-zone respiration and, in turn, some vegetation cover and therefore wetter conditions than present. This implication is also supported by the ^{10}Be depth profile model results. The calculated late Pliocene chert erosion rate of 14 m m.y.$^{-1}$ is an order of magnitude faster than that measured presently in chert bedrock in hyperarid deserts of Israel (Haviv et al., 2006). Next, aridity increased and calcic-gypsic and gypsic-salic soil horizons engulfed the calcic horizon. The soil development was accompanied by (1) the formation of a thick (~10 cm) Av horizon immediately underneath the well-developed, 1.5–1.9 Ma desert pavement and (2) the accumulation of very fine sand to clay dust below the Av horizon. The timing of pedogenic carbonate deposition is not well established. However, as mentioned already, Amit et al. (2006) showed that climatic conditions during the past 300 k.y., and perhaps since the early Pleistocene, have been too arid for soil carbonate deposition in the southern Negev; thus, the Bk horizon may be of early to middle Pleistocene age.

Our results indicate a late Pliocene to early Pleistocene surface age for the Paran Plains and similar surfaces in the Near East deserts. Model scenarios and results show that initial gravel deposition took place between ca. 2.35 Ma and ca. 2.05 Ma, and abandonment of the surface occurred 1.9–1.5 Ma. The abandonment was followed by Reg soil and extensive desert pavement formation. This history is in agreement with the geologic temporal framework

attributed to the Arava Formation, the sedimentary sequence deposited by the ancient Paran drainage system as it drained into the evolving Dead Sea basin (Avni, 1991; Avni et al., 2000). Cosmogenic isotope analyses have provided, for the first time, radiometric ages for this continental and otherwise undated formation.

CONCLUSIONS

Cosmogenic isotope measurements from the ancient desert pavements and Reg soils of the tectonically stable and hyperarid areas of the southern Negev indicate extreme geologic stability of vast alluvial surfaces. Such ancient surfaces are ubiquitous throughout the Middle East in similar tectonic and climatic conditions. The combination of long-term hyperaridity, absence of vegetation and bioturbation, and the rapid reduction of original chert and carbonate clasts to a full mosaic of pebble-size desert pavement has protected these surfaces from erosion, and they now form a most remarkably stable landscape on Earth, a landscape that essentially has not eroded for $>10^6$ yr.

The difference in cosmogenic dosing, and thus in the calculated exposure ages, of chert clasts in comparison with carbonate clasts is a consequence of the diffusion process that reduced the original bar and swale morphology of these alluvial surfaces. Even if we consider the maximum erosion rate implied by the carbonate samples (0.75–0.83 m m.y.$^{-1}$) operating throughout the history of the Paran Plain surface, we find surface lowering to be ~1–1.5 m. This may be the height difference between bars and swales.

The combination of field evidence, cosmogenic isotope concentrations, and OSL ages suggests that in the past several hundreds of thousands of years, erosion in the Paran Plain geomorphic system has been approaching nearly zero. Both the cumulative nature of the soil, which does not present any evidence of stripping, and the addition of material (as opposed to removal) to the system by slow eolian processes, suggest extreme stability. Furthermore, chert clasts, which compose the majority of the desert pavement, have been reduced to their minimal size, and pavement development has reached its peak and provides a most effective surface armor.

In the case of the Paran Plains, the amalgamating approach has yielded exceptional results. The reproducibility of cosmogenic nuclide concentration measurements within samples that were spatially separated exhibits the power of amalgamated samples in the investigation of surface processes. Other extremely old landscapes (i.e., the Atacama and Namib Deserts) should be dated considering our approach of amalgamation.

ACKNOWLEDGMENTS

We thank N. Teutsch, M. Harel, A. Lokshin, T. HaLevi, and D. Shtiber for laboratory assistance and inductively coupled plasma measurements. We thank J. Refael, J. Mizrahi, and R. Madmon for field assistance. We thank J. Gosse, M. Reheis, and an anonymous reviewer for excellent reviews and comments. This project was funded by the U.S. Army Research Office (DAAD19–03–1-0159) and by the United States–Israel Binational Science Foundation grant 2006–221.

REFERENCES CITED

Aitken, M.J., 1998, An Introduction to Optical Dating: Oxford, Oxford University Press, 267 p.

Amit, R., and Gerson, R., 1986, The evolution of Holocene Reg (gravelly) soils in deserts; an example from the Dead Sea region: Catena, v. 13, no. 1, p. 59–79, doi: 10.1016/S0341-8162(86)80005-4.

Amit, R., Gerson, R., and Yaalon, D.H., 1993, Stages and rate of the gravel shattering process by salts in desert Reg soils: Geoderma, v. 57, no. 3, p. 295–324, doi: 10.1016/0016-7061(93)90011-9.

Amit, R., Enzel, Y., and Sharon, D., 2006, Permanent Quaternary hyperaridity in the Negev, Israel, resulting from regional tectonics blocking Mediterranean frontal systems: Geology, v. 34, no. 6, p. 509–512, doi: 10.1130/G22354.1.

Avni, Y., 1991, The Geology, Paleogeography, and Landscape Evolution of the Negev Highlands and the Western Ramon Structure: Geological Survey of Israel Report GSI/6/91, 153 p.

Avni, Y., Bartov, Y., Garfunkel, Z., and Ginat, H., 2000, Evolution of the Paran drainage basin and its relation to the Plio-Pleistocene history of the Arava Rift western margin, Israel: Israel Journal of Earth Sciences, v. 49, p. 215–238, doi: 10.1560/W8WL-JU3Y-KM7W-8LX4.

Belton, D.X., Brown, R.W., Kohn, B.P., Fink, D., and Farley, K.A., 2004, Quantitative resolution of the debate over antiquity of the central Australian landscape: Implications for the tectonic and geomorphic stability of cratonic interiors: Earth and Planetary Science Letters, v. 219, p. 21–34, doi: 10.1016/S0012-821X(03)00705-2.

Bierman, P.R., 1994, Using in situ produced cosmogenic isotopes to estimate rates of landscape evolution; a review from the geomorphic perspective: Journal of Geophysical Research, ser. B, Solid Earth and Planets, v. 99, no. 7, p. 13,885–13,896, doi: 10.1029/94JB00459.

Bierman, P.R., and Caffee, M.W., 2001, Slow rates of rock surface erosion and sediment production across the Namib Desert and escarpment, southern Africa: American Journal of Science, v. 301, p. 326–358, doi: 10.2475/ajs.301.4-5.326.

Bierman, P.R., and Caffee, M.W., 2002, Cosmogenic exposure and erosion history of Australian bedrock landforms: Geological Society of America Bulletin, v. 114, no. 7, p. 787–803, doi: 10.1130/0016-7606(2002)114<0787:CEAEHO>2.0.CO;2.

Bierman, P.R., and Turner, J., 1995, ^{10}Be and ^{26}Al evidence for exceptionally low rates of Australian bedrock erosion and the likely existence of pre-Pleistocene landscapes: Quaternary Research, v. 44, p. 378–382, doi: 10.1006/qres.1995.1082.

Binnie, S.A., Spotila, J.A., Phillips, W.M., Summerfield, M.A., and Fifield, K., 2003, The coexistence of steady and non-steady state topography in the San Bernardino Mountains, southern California, from cosmogenic ^{10}Be and U-Th/ He thermochronology: Geological Society of America Abstracts with Programs, v. 35, no. 6, p. 63.

Birkeland, P.W., 1999, Soils and Geomorphology: New York, Oxford University Press, 430 p.

Briner, J.P., Swanson, T.W., and Caffee, M., 2001, Late Pleistocene cosmogenic ^{36}Cl glacial chronology of the southwestern Ahklun Mountains, Alaska: Quaternary Research, v. 56, p. 148–154, doi: 10.1006/qres.2001.2255.

Briner, J.P., Kaufman, D.S., Werner, A., Caffee, M., Levy, L., Manley, W.F., Kaplan, M.R., and Finkel, R.C., 2002, Glacier advance during the late glacial (Younger Dryas?) in the Ahklun Mountains, southwestern Alaska: Geology, v. 30, p. 679–682, doi: 10.1130/0091-7613(2002)030<0679:GRDTLG>2.0.CO;2.

Brown, E.T., Bourles, D.L., Burchfiel, B.C., Qidong, D., Jun, L., Molnar, P., Raisbeck, G.M., and Yiou, F., 1998, Estimation of slip rates in the southern Tien-Shan using cosmic ray exposure dates of abandoned alluvial surfaces: Geological Society of America Bulletin, v. 110, no. 3, p. 377–386, doi: 10.1130/0016-7606(1998)110<0377:EOSRIT>2.3.CO;2.

Calvo, R., and Bartov, Y., 2001, Hazeva Group, southern Israel; new observations, and their implications for its stratigraphy, paleogeography, and tectono-sedimentary regime: Israel Journal of Earth Sciences, v. 50, no. 2–4, p. 71–99, doi: 10.1560/B02L-6K04-UFQL-KUE3.

Chappell, J., Hongbo Zheng, and Fifield, K., 2006, Yangtse River sediments and erosion rates from source to sink traced with cosmogenic ^{10}Be: Sediments from major rivers: Palaeogeography, Palaeoclimatology, Palaeoecology, v. 241, p. 79–94.

Clapp, E.M., Bierman, P.R., Schick, A.P., Lekach, J., Enzel, Y., and Caffee, M., 2000, Sediment yield exceeds sediment production in arid region drainage basins: Geology, v. 28, no. 11, p. 995–998, doi: 10.1130/0091-7613(2000)28<995:SYESPI>2.0.CO;2.

Cooke, R.V., Warren, A., and Goudie, A.S., 1993, Desert Geomorphology: London, University College London Press, 526 p.

Daeron, M., Benedetti, L., Tapponnier, P., Sursock, A., and Finkel, R.C., 2004, Constraints on the post approximately 25 ka slip rate of the Yammouneh fault (Lebanon) using in situ cosmogenic ^{36}Cl dating of offset limestone clast fans: Earth and Planetary Science Letters, v. 227, no. 1–2, p. 105–119, doi: 10.1016/j.epsl.2004.07.014.

Dan, J., Yaalon, D.H., Moshe, R., and Nissim, S., 1982, Evolution of Reg soils in southern Israel and Sinai: Geoderma, v. 28, p. 173–202, doi: 10.1016/0016-7061(82)90002-7.

Dunai, T.J., 2000, Scaling factors for production rates of in situ produced cosmogenic nuclides: A critical reevaluation: Earth and Planetary Science Letters, v. 176, p. 157–169, doi: 10.1016/S0012-821X(99)00310-6.

Dunai, T.J., Gonzalez-Lopez, G.A., and Juez-Larre, J., 2005, Oligocene-Miocene age of aridity in the Atacama Desert by exposure dating of erosion-sensitive landforms: Geology, v. 33, no. 4, p. 321–324, doi: 10.1130/G21184.1.

Duncan, C.C., Masek, J.G., Bierman, P., Larsen, J., and Caffee, M., 2001, Extraordinarily high denudation rates suggested by ^{10}Be and ^{26}Al analysis of river sediments, Bhutan Himalaya: Geological Society of America Abstracts with Programs, v. 33, no. 6, p. A312.

Ewing, S.A., Sutter, B., Owen, J., Nishiizumi, K., Sharp, W., Cliff, S.S., Perry, K., Dietrich, W., McKay, C.P., and Amundson, R., 2006, A threshold in soil formation at Earth's arid–hyperarid transition: Geochimica et Cosmochimica Acta, v. 70, p. 5293–5322, doi: 10.1016/j.gca.2006.08.020.

Fink, D., and Smith, A., 2007, An intercomparison of ^{10}Be and ^{26}Al AMS reference standards and the ^{10}Be half-life: Nuclear Instruments and Methods in Physics Research, v. B259, p. 600–609.

Fogwill, C.J., Bentley, M.J., Sugden, D.E., Kerr, A.R., and Kubik, P.W., 2004, Cosmogenic nuclides ^{10}Be and ^{26}Al imply limited Antarctic ice sheet thickening and low erosion in the Shackleton Range for >1 m.y.: Geology, v. 32, no. 3, p. 265–268, doi: 10.1130/G19795.1.

Garfunkel, Z., and Horovitz, A., 1966, The upper Tertiary and Quaternary morphology of the Negev: Israel Journal of Earth Sciences, v. 15, p. 101–117.

Gerson, R., 1982, The Middle East; landforms of a planetary desert through environmental changes, *in* The Geological Story of the World's Deserts: Uppsala, Sweden, University of Uppsala, Department of Quaternary Geology, 11th INQUA congress, Moscow, USSR, Striae, v. 17, p. 52–78.

Gerson, R., and Amit, R., 1987, Rates and modes of dust accretion and deposition in an arid region: The Negev, Israel, *in* Fostick, L., and Reid, I., eds., Desert Sediments: Ancient and Modern: Geological Society of London Special Publication 35, p. 157–169.

Ginat, H., Zilberman, E., and Amit, R., 2002, Red sedimentary units as indicators of early Pleistocene tectonic activity in the southern Negev Desert, Israel,

in Drainage Basin Dynamics and Morphology: Geomorphology, v. 45, no. 1–2, p. 127–146, doi: 10.1016/S0169-555X(01)00193-3.

Gosse, J.C., and Phillips, F.M., 2001, Terrestrial in situ cosmogenic nuclides: Theory and application: Quaternary Science Reviews, v. 20, no. 14, p. 1475–1560, doi: 10.1016/S0277-3791(00)00171-2.

Gosse, J., McDonald, E., and Finkel, R., 2003a, Cosmogenic nuclide dating of arid region alluvial fans: Geological Society of America Abstracts with Programs, v. 35, no. 3, p. 8.

Gosse, J., McDonald, E., and Finkel, R., 2003b, Cosmogenic nuclide dating of arid region alluvial fans, *in* XVI INQUA Congress: Shaping the Earth; a Quaternary Perspective: Congress of the International Union for Quaternary Research, v. 16, p. 228.

Gosse, J., McDonald, E., Pederson, J., Stockli, D.F., Lee, J., Stockli, L.D., and Yang, G., 2004, Oxygen isotope stage 4 sediment dominates the U.S. Southwest alluvial record: Geological Society of America Abstracts with Programs, v. 36, no. 5, p. 307.

Gran-Mitchell, S.E., Matmon, A., Bierman, P.R., Rizzo, D., Enzel, Y., and Caffee, M., 2001, Determination of displacement history from a limestone normal fault scarp using cosmogenic ^{36}Cl, northern Israel: Journal of Geophysical Research, v. 106, no. B3, p. 4247–4264, doi: 10.1029/2000JB900373.

Haviv, I., Enzel, Y., Zilberman, E., Whipple, K., Stone, J., Matmon, A., and Fifield, L.K., 2006, Climatic control on erosion rates of dolo-limestone hilltops: Bet-Shean, The Israel Geological Society, Annual Meeting Abstract Book, p. 54.

Kober, F., Ivy-Ochs, S., Schlunegger, F., Baur, H., Kubik, P.W., and Wieler, R., 2007, Denudation rates and a topography-driven rainfall threshold in northern Chile: Multiple cosmogenic nuclide data and sediment yield budgets: Geomorphology, v. 83, p. 97–120, doi: 10.1016/j.geomorph.2006.06.029.

Lal, D., 1988, In situ–produced cosmogenic isotopes in terrestrial rocks: Annual Review of Earth and Planetary Sciences, v. 16, p. 355–388.

Matmon, A., Bierman, P., Larsen, J., Southworth, S., Pavich, M., and Caffee, M., 2003, Erosion of an ancient mountain range, the Great Smoky Mountains, North Carolina and Tennessee: American Journal of Science, v. 303, p. 817–855, doi: 10.2475/ajs.303.9.817.

Matmon, A., Schwartz, D., Finkel, R., Clemmens, S., and Hanks, T., 2005a, Dating offset fans along the Mojave section of the San Andreas fault using cosmogenic ^{26}Al and ^{10}Be: Geological Society of America Bulletin, v. 117, p. 795–807, doi: 10.1130/B25590.1.

Matmon, A., Shaked, Y., Porat, N., Enzel, Y., Finkel, R., Lifton, N., Boaretto, E., and Agnon, A., 2005b, Landscape development in a hyper arid sandstone environment along the margins of the Dead Sea fault: Implications from dated rock falls: Earth and Planetary Science Letters, v. 240, p. 803–817, doi: 10.1016/j.epsl.2005.06.059.

Matmon, A., Nichols, K.K., and Finkel, R., 2006, Isotopic insights into smoothening of abandoned fan surfaces, southern California: Quaternary Research, v. 66, p. 109–118, doi: 10.1016/j.yqres.2006.02.010.

McDonald, E.V., McFadden, L.D., and Wells, S.G., 2003, Regional response of alluvial fans to the Pleistocene-Holocene climatic transition, Mojave Desert, California, *in* Enzel, Wells, and Lancaster, eds., Paleoenvironments and Paleohydrology of the Mojave and Southern Great Basin Deserts: Geological Society of America Special Paper 368, p. 189–205.

McFadden, L.D., Wells, S.G., and Jercinovich, M.J., 1987, Influences of eolian and pedogenic processes on the origin and evolution of desert pavements: Geology, v. 15, p. 504–508, doi: 10.1130/0091-7613(1987)15<504:IOEAPP>2.0.CO;2.

McFadden, L.D., Wells, S.G., Eppes, M.C., and Gillespie, A.R., 2000, The evolution of desert piedmont surfaces; studies of the origin of desert pavements and soils: Geological Society of America Abstracts with Programs, v. 32, no. 7, p. 222.

Milliman, J.D., and Syvitski, P.M., 1992, Geomorphic/tectonic control of sediment discharge to the ocean: The importance of small mountainous rivers: The Journal of Geology, v. 100, p. 525–544.

Murray, A., and Wintle, A.G., 2000, Luminescence dating of quartz using an improved single-aliquot regenerative-dose protocol: Radiation Measurements, v. 32, p. 57–73, doi: 10.1016/S1350-4487(99)00253-X.

Nishiizumi, K., Caffee, M.W., Finkel, R.C., Brimhall, G., and Mote, T., 2005, Remnants of a fossil alluvial fan landscape of Miocene age in the Atacama Desert of northern Chile using cosmogenic nuclide exposure age dating: Earth and Planetary Science Letters, v. 237, no. 3–4, p. 499–507, doi: 10.1016/j.epsl.2005.05.032.

Nishiizumi, K., Imamura, M., Caffee, M.W., Southon, J.R., Finkel, R.C., and McAninch, J., 2007, Absolute calibration of ^{10}Be AMS standards: Nuclear Instruments and Methods in Physics Research, v. B258, p. 403–413.

Pelletier, J.D., Cline, M., and DeLong, S.B., 2007, Desert pavement dynamics: Numerical modeling and field based calibration: Earth Surface Processes and Landforms, v. 32, p. 1913–1927, doi: 10.1002/esp.1500.

Phillips, F.M., Stone, W.D., and Fabryka Martin, J.T., 2001, An improved approach to calculating low-energy cosmic-ray neutron fluxes near the land/atmosphere interface: Chemical Geology, v. 175, no. 3–4, p. 689–701.

Phillips, W.M., McDonald, E.V., Reneau, S.L., and Poths, J., 1998, Dating soils and alluvium with cosmogenic ^{21}Ne depth profiles; case studies from the Pajarito Plateau, New Mexico, USA: Earth and Planetary Science Letters, v. 160, no. 1–2, p. 209–223, doi: 10.1016/S0012-821X(98)00076-4.

Quade, J., 2001, Desert pavements and associated rock varnish in the Mojave Desert; how old can they be?: Geology, v. 29, no. 9, p. 855–858, doi: 10.1130/0091-7613(2001)029<0855:DPAARV>2.0.CO;2.

Rabikovitch, S., Pines, F., Dan, J., 1957, Soils of the Central and Southern Negev, Final report, Ford Foundation Research Project, p. 211–238.

Repka, J.L., Anderson, R.S., and Finkel, R.C., 1997, Cosmogenic dating of fluvial terraces, Fremont River, Utah: Earth and Planetary Science Letters, v. 152, p. 59–73, doi: 10.1016/S0012-821X(97)00149-0.

Safran, E.B., Bierman, P.R., Aalto, R., Dunne, T., Whipple K.X., and Caffee, M., 2005, Erosion rates driven by channel network incision in the Bolivian Andes: Earth Surface Processes and Landforms, v. 30, p. 1007–1024.

Schaller, M., von Blanckenberg, F., Hovius, N., and Kubik, P.W., 2001, Large-scale erosion rates from in situ–produced cosmogenic nuclides in European river sediments: Earth and Planetary Science Letters, v. 188, p. 441–458.

Siame, L.L., Bourlès, D.L., Sébrier, M., Bellier, O., Castano, J.C., Araujo, M., Perez, M., Raisbeck, G., and Yiou, M., 1997, Cosmogenic datings of alluvial fans along the Central Andes El Tigre fault (Argentina): Paleoclimatic and tectonic implications: Geology, v. 25, p. 975–978, doi: 10.1130/0091-7613(1997)025<0975:CDRFTK>2.3.CO;2.

Small, E.E., Anderson, R.S., and Hancock, G.S., 1999, Estimates of the rate of regolith production using ^{10}Be and ^{26}Al from an alpine hillslope, *in* Harbor, ed., Cosmogenic Isotopes in Geomorphology: Geomorphology, v. 27, no. 1–2, p. 131–150, doi: 10.1016/S0169-555X(98)00094-4.

Steinitz, G., and Bartov, Y., 1991, The Miocene-Pliocene history of the Dead Sea segment of the rift in light of K-Ar ages of basalts: Israel Journal of Earth Sciences, v. 40, no. 1–4, p. 199–208.

Stone, J., 2000, Air pressure and cosmogenic isotope production: Journal of Geophysical Research, v. 105, no. B10, p. 23,753–23,759, doi: 10.1029/2000JB900181.

Stone, J.O., Allan, G.L., Fifield, L.K., and Cresswell, R.G., 1996, Cosmogenic chlorine-36 from calcium spallation: Geochimica et Cosmochimica Acta, v. 60, no. 4, p. 679–692, doi: 10.1016/0016-7037(95)00429-7.

Stone, J., Evans, J.M., Fifield, L.K., Allan, G.L., and Cresswell, R.G., 1998, Cosmogenic chlorine-36 production in calcite by muons: Geochimica et Cosmochimica Acta, v. 62, no. 3, p. 433–454, doi: 10.1016/S0016-7037(97)00369-4.

Stone, J., Cowdery, S.G., Finkel, R.C., Balco, G., Sugden, D., and Sass, L.C., 2005, Exposure history of intermittently-glaciated nunataks in the Ford Ranges, West Antarctica: Geological Society of America Abstracts with Programs, v. 37, no. 7, p. 399.

Summerfield, M.A., Stuart, F.M., Cockburn, H.A.P., Sugden, D.E., Denton, G.H., Dunai, T., and Marchant, D.R., 1999, Long-term rates of denudation in the Dry Valleys, Transantarctic Mountains, southern Victoria Land, Antarctica, based on in-situ–produced cosmogenic ^{21}Ne, *in* Harbor, ed., Cosmogenic Isotopes in Geomorphology: Geomorphology, v. 27, no. 1–2, p. 113–129, doi: 10.1016/S0169-555X(98)00093-2.

Valentine, G.A., and Harrington, C.D., 2006, Clast size controls and longevity of Pleistocene desert pavements at Lathrop Wells and Red Cone Volcanoes, southern Nevada: Geology, v. 34, no. 7, p. 533–536, doi: 10.1130/G22481.1.

Vanacker, V., von Blanckenburg, F., Hewawasam, T., and Kubik, P.W., 2007, Constraining landscape development of the Sri Lankan escarpment with cosmogenic nuclides in river sediment: Earth and Planetary Science Letters, v. 253, p. 402–414, doi: 10.1016/j.epsl.2006.11.003.

Vance, D., Bickle, M., Ivy-Ochs, S., and Kubick, P.W., 2003, Erosion and exhumation in the Himalaya from cosmogenic isotope inventories of river sediments: Earth and Planetary Science Letters, v. 206, p. 273–288, doi: 10.1016/S0012-821X(02)01102-0.

Wells, S.G., McFadden, L.D., Poths, J., and Olinger, C.T., 1995, Cosmogenic ^{3}He surface-exposure dating of stone pavements; implications for landscape evolution in deserts: Geology, v. 23, p. 613–616, doi: 10.1130/0091-7613(1995)023<0613:CHSEDO>2.3.CO;2.

Willett, S.D., Fisher, D., and Yeh-En-Chao, 2001, High erosion rates in Taiwan from apatite and zircon fission track ages, *in* Earth System Processes: The Geological Society of America and the Geological Society of London, International, Programs with Abstracts, p. 96.

Zilberman, E., and Avni, Y., 2006, The Hemar conglomerate—The relics of a drainage system that drained the trans-Jordanian region to the Mediterranean through the Beer-Sheva channel: Neve Zohar, The Israel Geological Society, Annual Meeting Field Guide, p. 37–53 (in Hebrew).

Zilberman, E., Amit, R., Heimann, A., and Porat, N., 2000, Changes in Holocene paleoseismic activity in the Hula pull-apart basin, northern Dead Sea Rift, Israel: Tectonophysics, v. 321, p. 237–252, doi: 10.1016/S0040-1951(00)00035-4.

Manuscript Received 26 February 2008
Revised Manuscript Received 15 July 2008
Manuscript Accepted 28 July 2008

Printed in the USA